THE AMERICAN SOCIETY OF MECHANICAL ENGINEERS
345 E. 47th St., New York, N.Y. 10017

96-GT-511

TRANSONIC STALL/CHOKE FLUTTER ANALYSIS OF CASCADES BY A NAVIER-STOKES SOLUTION-ADAPTIVE APPROACH

C. J. Hwang and J. M. Fang
Institute of Aeronautics and Astronautics
National Cheng Kung University
Tainan, Taiwan, Republic of China

ABSTRACT

In this paper, the stall and choke flutter analyses of NACA 0006 unstaggered cascades in transonic viscous flows are presented by using a time domain approach. For the present time domain approach, a solution-adaptive finite volume method with rigid-deformable dynamic mesh treatment is adopted to solve the two-dimensional unsteady Navier-Stokes equations. The structural model equations, where each blade is treated as a typical section having plunging and pitching degrees of freedom, are integrated to obtain the blade displacements by an explicit four-stage Runge-Kutta scheme. In the present calculations, the Baldwin-Lomax turbulence model and two transition formulations are used. The instantaneous meshes, vorticity contours, pressure contours and velocity vectors around the trailing edge clearly indicate the flow phenomena, such as the vortex shedding and λ shocks with separation bubbles. From the histories of blade displacements and total energy, the flutter phenomena are studied. Furthermore, the Fast Fourier Transformation (FFT) and modal identification techniques are introduced to investigate the aeroelastic behaviors in present transonic stall and choke flutter problems.

INTRODUCTION

Because the flow-induced vibrations may cause blade failure, the aeroelastic instability is considerably important in the development of turbomachines. Blade vibrations are generally classified into self-excited vibration (flutter) and forced vibration. In the present work, the viscous transonic cascade flutter problems are studied. For the cascade flutter in transonic flow, the shocks move along the blade surface in response to the blade motion. Also, the shock strength is changed and possibly vanishes over the time. These shock waves reduce the efficiency of turbomachines through total pressure losses, and may make the boundary layer separation on the blade surfaces. Therefore, the effect of shock waves/boundary layer interaction should be considered in the turbomachinery design. According to the descriptions given by Dowell et al. (1989), the stall flutter may occur at operation near the surge line and will be limited to operate at higher than average incidence. For a multistage compressor, there is a possible presence of choke flutter in the middle stages operating at lower than average incidence or negative incidence. Until now, the transonic stall and choke flutter phenomena and mechanisms are not completely understood. Therefore, the continued study in those two kinds of flutter problems is necessary and worthwhile.

In the past decades, several papers have been presented to discuss the characteristics of stall/choke flutter of cascades. El-Aini et al. (1986) investigated the subsonic/transonic stall flutter of an advanced low pressure compressor. To be flutter-free for this compressor over its entire flight envelope, this paper showed that the continued research in transonic unsteady aerodynamics was needed, particulary, the effects of passage shocks and large leading edge incidence. For the incompressible flow past a cascade of airfoils, Sisto et al. (1991) used a scheme, which was based on a modified form of the vortex method, to study the stall flutter phenomena. In this paper, the airfoils were modeled structurally as single-degree-freedom linear oscillators. Because a stall flutter in cascade occurs with a coupled bending-torsion mode, they also showed that a study of the two-degrees-of-freedom case was mandatory. For the choke flutter, the experimental results (Tanida and Saito, 1977; Jutras et al., 1980) and analytically-based predictions (Micklow and Jeffers, 1981) were presented. Tanida and Saito (1977) evaluated the possibility of the choke flutter in a transonic cascade operating under choking conditions. Jutras et al. (1980) conducted a systematic and controlled experiment to investigate negative incidence choke flutter in a non-rotating annular cascade vehicle. Based on a semi-actuator disk theory, Micklow and Jeffers (1981) presented a mathematical analysis for the oscillating cascade of airfoils in choked flow. As mentioned in this reference,

Presented at the International Gas Turbine and Aeroengine Congress & Exhibition
Birmingham, UK — June 10-13, 1996

this semi-actuator model was useful as a conservative choke flutter design system, but it was limited to interblade phase angles of ±90 deg.

Due to the significant progress in computational fluid dynamics, many numerical procedures are applied to study the cascade flutter problems. In the numerical analysis of inviscid transonic cascade flutter, the frequency domain (Reddy et al., 1991; Bakhle et al., 1992) and time domain (Reddy et al., 1991; Bakhle et al., 1992; Bendiksen and Hsiao, 1993) approaches have been widely used. Even though those inviscid flutter analyses have provided several wonderful results, the viscous effects, which are important in the stall/choke flutter, are neglected. To treat the viscous flutter problems, one of the way is to solve the Navier-Stokes equations. Siden (1991) used the Navier-Stokes solver to study the aerodynamic coefficients and flow behaviors for the subsonic compressor cascade, where the motion of each blade was known. As mentioned by Siden (1991), the viscous effects due to the regions of separated flow could be of major importance in the case of blade flutter predictions. He and Denton (1994) developed a time-marching method to solve the three-dimensional thin-layer Navier-Stokes equations in transonic rotor blade flutter calculations. The calculated unsteady loadings due to oscillations of rotor blades demonstrated some remarkable three-dimensional viscous flow features. The torsion mode flutter stability was determined hy the imaginary part of the unsteady aerodynamic moment coefficient. In the aforementioned two papers, the aerodynamic codes are executed for prescribed blade motions and then carry out blade flutter analyses. In other words, no structural model equations are considered in the above-mentioned two papers. To more accurately and reasonably investigate the transonic stall/choke flutter of cascades, it is suggested to solve the equations of motion for the blade and fluid simultaneously in time. Furthermore, a scheme having the solution-adaptive capability is preferred because the complex unsteady flow phenomena, such as the interaction of shock and boundary layer or the vortex shedding, occur in the present two kinds of flutter problems.

The objective of this work is to investigate the stall and choke flutter behaviors of cascades in transonic viscous flows by using a time domain approach. The two-dimensional unsteady Navier-Stokes equations and the structural model equations are integrated simultaneously in time. For the aerodynamic solver, a Navier-Stokes solution-adaptive approach (Hwang and Fang, 1995b) is adopted. This approach includes a finite volume method, a rigid-deformable dynamic mesh algorithm and a mesh-refinement technique. For the structural solver, an explicit four-stage Runge-Kutta scheme is used. By combining the aerodynamic and structural solvers, the unstaggered NACA 0006 transonic cascade flows with an interblade phase angle (σ) of 180° and with four blades are employed to study the stall and choke flutter phenomena. Based on the computed solutions and the related analyses by the FFT and modal identification techniques, the unsteady flow phenomena and aeroelastic behaviors are investigated.

NUMERICAL FORMULATION

Aerodynamic Model

In this paper, the two-dimensional unsteady Navier-Stokes equations with moving cell effects (Hwang and Yang, 1994) are solved in the X-Y Cartesian coordinate system. An algebraic eddy-viscosity turbulent formulation, which was presented by Baldwin and Lomax (1978), is adopted. For the transition region that exists between a laminar and turbulent flow, the transition location and intermittency factor are accounted. The formulations, which were predicted by Abu-Ghannam and Shaw (1980) for the natural transition (low free-stream turbulence) in an attached flow and given by Mayle (1991) for the transition in the separated flow, respectively, are used. In the present computations, a numerical viscous flux formulation (Hwang and Yang, 1994), where the first-order derivatives of the velocity components and temperature were calculated by constructing auxiliary cells and using the Green's theorem for surface intergation, is incorporated with the locally implicit cell-centered finite volume Total-Variation-Diminishing (TVD) solution-adaptive approach (Hwang and Fang, 1995a) on quadrilateral-triangular meshes. The descriptions and evaluations of present numerical approach were given in detail by Hwang and Fang (1995b).

To adjust the meshes with the moving and oscillating blades in time, a rigid-deformable dynamic mesh algorithm (Hwang and Yang, 1994) is introduced. For this rigid-deformable dynamic mesh algorithm, a layer of O-typed quadrilaterals, which is generated around each blade surface, is moved and oscillated rigidly with respect to its own blade. Then, the triangles, which are distributed elesewhere in the flow region, are treated by a dynamic mesh technique. By using this rigid-deformable dynamic mesh algorithm, the orthogonality on each blade surface and the smoothness of quadrilateral-triangular meshes are maintained. Besides the aforementioned dynamic mesh algorithm, the mesh-refinement technique (Hwang and Fang, 1995a) is employed, so that the meshes can be automatically refined during the unsteady calculations. For this mesh-refinement technique, a coarse mesh is used as a background grid, and a two-level refinement procedure is employed. In the present technique, the enrichment indicator $|\nabla\rho|$ is adopted, and two values of $C1$ and $C2$ are chosen to determine two threshold values, respectively. In general, the values of $C1$ and $C2$ are dependent on the flow feature and the numbers of background cells to be refined during the computations. By applying the mesh-refinement procedure to the present flutter calculations in a simple way, the values of $C1$ and $C2$ are kept constant and set to be 0.3 and 0.8, respectively. Also, the grid adaption is started when the aeroelastic behavior, such as flutter or stable situations, is observed during the calculations.

In the present flutter calculations, the steady-state solutions are used as initial conditions. For the steady-state computations, the adiabatic wall and no-slip conditions are imposed on the blade surfaces. The pressure and density at the blade surfaces are extrapolated from the values at the interior cells. About the inlet plane, the one-dimensional characteristic analysis is adopted. On the exit boundary, the back pressure is prescribed, and the other flow properities are extrapolated from those at the interior cells. In the flutter calculations with dynamic mesh

effects, the value of flow velocity on the blade surface is equal to the grid speed of the boundary cell on the moving blade. Pressure and density are obtained from the values at the interior cells. At the inlet and exit planes, the one-dimensional unsteady boundary conditions (Giles, 1990) are adopted. In the flutter calculations of cascade with $\sigma = 180°$, the symmetric treatment is applied on upper and lower boundaries of the computational domain (Fig. 1a). Therefore, the single blade is utilized in place of two blades. As for the spatially periodic boundaries of cascade with four blades (Fig. 1b), the numerical treatment in the steady and unsteady calculations is same as that presented by Hwang and Yang (1994).

Structural Model

In the present work, each blade of a cascade is modeled as a typical section with plunging (h, positive down) and pitching (α, postive clockwise) degrees of freedom. The structural damping is not considered. By introducing a non-dimensional time $\tau = \frac{ta_\infty}{2b}$, the non-dimensional form of equations of motion for the typical section is expressed as:

$$[M]\{\ddot{q}\} + [K]\{q\} = \{F\} \tag{1}$$

where

$$[M] = \begin{bmatrix} 1 & \frac{x_\alpha}{2} \\ \frac{x_\alpha}{2} & \frac{r_\alpha^2}{4} \end{bmatrix}, [K] = \begin{bmatrix} 4M_\infty{}^2 k_h{}^2 & 0 \\ 0 & M_\infty{}^2 r_\alpha{}^2 k_\alpha{}^2 \end{bmatrix} \tag{2}$$

and

$$[q] = \begin{bmatrix} \frac{h}{2b} \\ \alpha \end{bmatrix}, [F] = \begin{bmatrix} \frac{-2M_\infty{}^2 C_l}{\pi\mu} \\ \frac{2M_\infty{}^2 C_m}{\pi\mu} \end{bmatrix} \tag{3}$$

In the above equations, the dots over q indicate differentiation with respect to time, and b is the semi-chord. Noted that, $x_\alpha = \frac{S_\alpha}{mb}$ is the distance between the elastic axis (E.A.) and center of mass in semi-chord units, and $r_\alpha = (\frac{I_\alpha}{mb^2})^{\frac{1}{2}}$ is the radius of gyration about the E.A. in semi-chord units. S_α and I_α are the static moment and moment of inertia per unit span about the E.A., and m is the mass of the typical section per unit span. C_l and C_m are the lift and moment coefficients, and $\mu = \frac{m}{\pi\rho b^2}$ is the mass ratio. By indicating that K_h and K_α are the spring constants for the plunging and pitching, $\omega_h = (\frac{K_h}{m})^{\frac{1}{2}}$ and $\omega_\alpha = (\frac{K_\alpha}{I_\alpha})^{\frac{1}{2}}$ are the uncoupled plunging and pitching natural frequencies. $k_h = \frac{\omega_h b}{U_\infty}$ and $k_\alpha = \frac{\omega_\alpha b}{U_\infty}$ are the plunging and pitching reduced frequencies.

By using $V^* = \frac{U_\infty}{b\omega_\alpha}$ as the reduced velocity, the matrix $[K]$ in Eq. (2) can be rewritten as:

$$[K] = \begin{bmatrix} \left(\frac{2M_\infty \omega_h}{V^* \omega_\alpha}\right)^2 & 0 \\ 0 & \left(\frac{M_\infty r_\alpha}{V^*}\right)^2 \end{bmatrix} \tag{4}$$

The total energy (E_{tot}) of each blade is expressed as :

$$E_{tot} = \frac{1}{2}\{\dot{q}\}^T[M]\{\dot{q}\} + \frac{1}{2}\{q\}^T[K]\{q\} \tag{5}$$

To obtain the structural displacements, $\frac{h}{2b}$ and α, the Eq. (1) is rewritten into first-order ordinary differential equations. Then, an explicit four-stage Runge-Kutta scheme is applied to solve those differential equations. For the present time-domain approach, the steady-state solutions of Navier-Stokes equations are chosen as the initial conditions, and a blade is given a small pitching velocity. Later on, the fluid and structural equations are simultaneously integrated in time. Therefore, the aerodynamic loads drive the structural equations, and the resulting structural displacements vary the aerodynamic loads during the flutter calculations. In the present flutter calculations, the maximum value of CFL (Courant-Friendrichs-Lewy) number is equal to 5.0 at every time-step, and the value of Reynolds number is chosen to be 1×10^6.

RESULTS AND DISCUSSION

Transonic Stall Flutter

To investigate the transonic stall flutter phenomena, two cascade problems are studied. For the first problem, an unstaggered NACA 0006 transonic cascade flow with an interblade phase angle (σ) of 180° is computed. The geometry, flow conditions and structural parameters are same as those presented by Bendiksen and Hsiao (1993) in inviscid transonic flutter analysis. In this case, a cascade gap-to-chord ratio ($\frac{s}{c}$) of 1.0, a mass ratio (μ) of 192, a ratio of natural frequencies in plunging and pitching ($\frac{\omega_h}{\omega_\alpha}$) of 1.0 and the elastic axis at 38% chord are employed. The upstream and downstream distances away from the blade are set to be three and four times chord-length (c). When the values of M_∞, $\frac{p_e}{p_\infty}$ (exit pressure ratio) and α_∞ (angle of attack) are equal to 0.85, 1.1 and 13°, the steady-state solution on the coarse mesh (Fig. 1a) is obtained. Under this condition, the blade is on the verge of stall that reaches the maximum static lift coefficient. Given an initial pitching velocity ($d\alpha/d\tau$) of 0.0425, the flutter calculations for two kinds of reduced velocities ($V^* = 2.5$ and 3.33) are processed. The coarse mesh shown in Fig. 1a is used as a background grid. For the case with $V^* = 3.33$, the mesh refinement is started at the time point (T) of 50. At six points in time, the instantaneous meshes, vorticity contours, pressure contours and velocity vectors around the trailing edge are plotted in Fig. 2. From those results, it is obvious that the flow field is essentially nonlinear. The vorticity contours (Fig. 2b) indicate the trailing-edge vortex shedding and the time-variation of the regions with high gradient of vorticity. In this case, those regions are located around the shocks, lower surface of blade, leading and trailing edges. As shown in Figs. 2c and 2d, the unsteady shock/boundary-layer behaviors including λ shocks with separation bubbles are clearly observed. To understand the aeroelastic behaviors, the time histories of α, $\frac{h}{c}$ and E_{tot} are plotted in Fig. 3. For those two kinds of flutter calculations, the amplitudes of $\frac{h}{c}$ and E_{tot} progressively increase, while the values of α first decrease then increase as the stall flutter occurs. Besides the above discussion, it is interesting to investigate the relationship of flow phenomena to the blade displacements. At T equal to 54 and 66, where the values of $\frac{h}{c}$ are nearly identical but different values of α exist (Fig. 3), the flow results shown in Fig. 2 are similar. Considering the status with same values of α but different values of $\frac{h}{c}$ (T = 58

and 72, Fig. 3), the vortex-shedding or shock/boundary-layer interaction, including separation bubble appears or becomes serious when T is equal to 72 (Fig. 2). From the above discussion, besides the torsion mode, the bending mode should be considered also for the transonic stall flutter problems. To obtain the frequencies and amplitudes of the responses, the FFT analysis of the blade displacements (α and $\frac{h}{c}$) is employed. The amplitudes are normalized by the maximum amplitudes of corresponding blade displacements. As shown in Fig. 4a ($V^* = 3.33$, $k_\alpha \approx 0.3$ and $k_h \approx 0.3$), the value of responding reduced frequency of the fundamental instability (f_0) for α or $\frac{h}{c}$ is a value of 0.24. With regard to the case with $V^* = 2.5$ ($k_\alpha = 0.4$ and $k_h = 0.4$), the value of fundamental frequency (f_0) for α or $\frac{h}{c}$ is equal to 0.36 (Fig. 4b). From the distributions of normalized amplitudes of blade displacements (Fig 4a), the sidebands ($\frac{3f_0}{4}$, $\frac{5f_0}{4}$, $\frac{3f_0}{2}$ $\cdots$), subharmonics ($\frac{f_0}{2}$ and $\frac{f_0}{4}$) and first ($2f_0$), second ($4f_0$) and higher harmonics in $V^* = 3.33$ case are negligible. Therefore, the aeroelastic behavior of transonic stall flutter of cascade is almost dominated by the fundamental instability. As shown in Fig. 4b ($V^* = 2.5$), no subharmonics are observed, and the amplitudes of first, second and higher harmonics are smaller. However, a significant response of frequency $\frac{6f_0}{5}$ for the plunging motion should be considered. By using the modal identification analysis (Bennett and Desmarais, 1975), the damping of the blade displacements can be estimated, and the flutter reduced velocity is defined when the largest damping vanishes. Based on the modal identification analysis and an extrapolation process, the flutter reduced velocity of transonic stall flutter in the present cascade with $\sigma = 180°$ is the value of $V_F^* = 2.0$. In the computation of stall flutter with $V^* = 3.33$, the average value of the time step (ΔT) is about 4.8×10^{-5}. Therefore, it takes about 2.56×10^5 time steps and 327 CPU hours to complete per cycle of motion on the HP 9000/700/735 workstation.

Subsequently, the NACA 0006 cascade with four blades is adopted to investigate the transonic stall flutter behaviors. The computational domain comprises four NACA 0006 blades (Fig. 1b), where the geometry, flow conditions and structural parameters of each blade are same as those presented in the aforementioned case ($V^* = 3.33$). In this flutter calculation, the lowest blade is given a small initial pitching velocity ($d\alpha/d\tau$) of 0.0425, and all the other blade displacements and velocities are initially zero. When the time point (T) is equal to 32, the coarse mesh (Fig. 1b) is automatically enriched by using the present solution-adaptive approach. The instantaneous meshes, vorticity contours and pressure contours at six points in time are plotted in Fig. 5. From the results presented in Figs. 5a and 5c, the formation, migration, strengthening and attenuation of shocks and shock/boundary-layer interaction, such as the λ shocks, are observed. As shown in Fig. 5b, the shedding of vortices around the trailing edge happens first at the lowest blade ($T = 58$), then it occurs at the second blade when T is equal to 74. The vorticity contours around the third and highest blades do not change much at the first three points in time. Instead of locating around the lower surface of blade for the case with $\sigma = 180°$ (Fig. 2), the high gradient of vorticity occurs above the upper surface of blade in the present case. As shown in Fig. 6, the amplitudes of $\frac{h}{c}$ and E_{tot} for the four blades, especially for the lowest and second blades, progressively increase. Unlike the transonic stall flutter of cascade with $\sigma = 180°$ (Fig. 3), the amplitudes of α continue to grow without decay during the time. Therefore, the stall flutter yields in this case. Based on the FFT analysis of the lowest blade displacements (Fig. 4c), the responding reduced frequency of the fundamental instability (f_0) for α or $\frac{h}{c}$ is equal to 0.34. Comparing with the results shown in Fig. 4a, there is a significant response of frequency $\frac{6f_0}{5}$ for the plunging motion in the present transonic stall flutter behavior of cascade with four blades. Therefore, the aeroelastic behavior is not completely dominated by the fundamental instability. In this case, the average value of ΔT is about 4.9×10^{-5}, and it takes about 2.51×10^5 time steps and 281 CPU hours to complete per cycle of motion on the DEC ALPHA 200 4/233 workstation.

Transonic Choke Flutter

For the transonic choke flutter problems, two kinds of NACA 0006 unstaggered cascades, which were utilized in the study of transonic stall flutter, are adopted again. First, the cascade of blades with an interblade phase angle (σ) of 180° is considered. On a coarse mesh (Fig. 1a), the steady-state solution is obtained when the values of M_∞, $\frac{p_s}{p_\infty}$ and α_∞ are equal to 0.85, 1.07 and $-5°$, respectively. Under this condition, the cascade flow is choked. It is the same as the transonic stall flutter calculations that two values of V^* (2.5 and 3.33) are used. During the solution-adaptive computation with $V^* = 3.33$, the mesh refinement is started at the time point (T) of 44. At six points in time, the instantaneous meshes, vorticity contours, pressure contours and velocity vectors around the trailing edge are plotted in Fig. 7. In response to the blade motion, the locations/strengthes of the λ shocks and separation bubbles shown in Figs. 7c and 7d are changed. It is the same as the stall flutter case (Fig. 2b) that the regions with high gradient of vorticity are located around lower surface of blade, shocks, leading and trailing edges. However, the vortex-shedding phenomenon is not observed in the present problem. To understand the aeroelastic behaviors, the time histories of α, $\frac{h}{c}$ and E_{tot} of the blade are plotted in Fig. 8. For the case with V^* equal to 3.33, the values of E_{tot} and oscillating amplitudes of α and $\frac{h}{c}$ increase with time. Therefore, the blade flutter occurs. If the value of V^* is replaced by 2.5, the amplitudes of α first decrease, then increase as the choke flutter happens. Moreover, the histories of $\frac{h}{c}$ and E_{tot} indicate that the blade is subject to the flutter. Besides the above discussion, it is interesting and worthwhile to investigate the relationship of choke flutter phenomena to the blade displacements. From the histories of blade displacements (α and $\frac{h}{c}$) shown in Fig. 8, the blade is moving up (bending) and also pitching (torsion) in the counter-clockwise direction at T equal to 44, 56 or 66. At those points in time, the λ shock with separation bubble appear near the trailing edge of upper surface of blade (Figs. 7c and 7d). When T is equal to 48 or 60, the blade is moving down and also pitching in the clockwise direction (Fig. 8). At those points in time, the λ shock with

separation bubble occurs near the trailing edge of lower surface of blade. However, the λ shock with separation bubble is located near the trailing edge of upper surface of blade when the blade is moving up but pitching in the clockwise direction (T = 52, Fig. 8). Therefore, it is the same as the discussion of stall flutter case that the bending and torsion modes should be considered simultaneously in the study of choke flutter problem. From the FFT output of the blade displacements (Fig. 9a), the responding reduced frequency of the fundamental instability (f_0) for α or $\frac{h}{c}$ is equal to 0.27 when the value of V^* is equal to 3.33. For the case with $V^* = 2.5$, the value of fundamental frequency (f_0) for α or $\frac{h}{c}$ is equal to 0.38 (Fig. 9b). It is the same as the discussion for the stall flutter of cascade with $\sigma = 180°$ that the aeroelastic behavior of present transonic choke flutter with $V^* = 3.33$ is almost controlled by the fundamental instability (Fig. 9a). The response of frequency $\frac{6f_0}{5}$ for the plunging motion in the case with $V^* = 2.5$ is significant (Fig. 9b). Based on the modal identification analysis and an extrapolation process, the flutter reduced velocity of present transonic choke flutter of cascade with $\sigma = 180°$ is found to be 2.2. In the computation of choke flutter with $V^* = 3.33$, the average value of ΔT is about 4.9×10^{-5}. Therefore, it takes about 2.51×10^5 time steps and 351 CPU hours to complete per cycle of motion on the DEC ALPHA 3000/400 workstation.

Finally, the NACA 0006 unstaggered cascade with four blades is employed to investigate the transonic choke flutter behaviors. On a coarse mesh (Fig. 1h), the flutter computation is processed only for $V^* = 3.33$, and the mesh refinement begins at the time point (T) of 24. At six points in time, the instantaneous meshes, vorticity contours and pressure contours are plotted in Fig. 10. From those results, the choking flowfields within some passages are clearly observed. During the time, the chock condition for each flow passage is changed. At some instant time (for example, T = 62), the λ shock appears around the trailing edge of lower surface of the lowest blade. Comparing the results presented in Fig. 5b, the vortex shedding phenomenon is not detected in this case. Also, the region with high gradient of vorticity is close to the blade surface. It is the same as the results of stall flutter problem (Fig. 5) that the gradient of vorticity around the shock, leading and trailing edges is larger than that of middle part of flow passage. According to the time histories of α, $\frac{h}{c}$ and E_{tot} (Fig. 11), the four blades are unstable. However, it is interesting to mention that the second blade is less unstable than the third and highest blades. This behavior is different from that of stall flutter case (Fig. 6). To understand the aeroelastic behaviors, the FFT analysis of lowest blade displacements (Fig. 9c) is performed. The value of responding reduced frequency of the fundamental instability (f_0) for α or $\frac{h}{c}$ is equal to 0.34. Comparing with the results shown in Fig. 4c, the value of f_0 is same for both kinds of flutter of cascade with four blades. However, the distributions of normalized amplitudes of blade displacements are different each other (Figs. 4c and 9c). For this choke flutter, the instabilities ($\frac{f_0}{3}$, $\frac{2f_0}{3}$, $\frac{4f_0}{3}$ $\cdots$) exist, but the magnitudes are negligible. Therefore, the transonic choke flutter behavior of cascade with four blades can be determined by the fundamental instability. In this case, the average value of ΔT is about 5×10^{-5}, and it takes about 2.5×10^5 time steps and 180 CPU hours to complete per cycle of motion on the DEC ALPHA 3000/700 workstation.

CONCLUSIONS

By using a time domain approach, the viscous transonic stall and choke cascade flutter phenomena are investigated in this paper. About the present time domain approach, the two-dimensional unsteady Navier-Stokes equations in conjunction with the turbulence and transition models are solved by a solution-adaptive finite volume method, and the structural model equations are integrated in time by the explicit four-stage Runge-Kutta scheme. In the present work, the NACA 0006 unstaggered cascades with an interblade phase angle (σ) of 180° or with four blades are adopted. For the transonic stall flutter with $\sigma = 180°$ and $V^* = 3.33$, the instantaneous meshes, pressure contours and velocity vectors around the trailing edge clearly show the shock/boundary-layer interaction, such as the λ shocks with separation bubbles. Also, the vorticity contours indicate the trailing-edge vortex shedding and the time-variation of the regions of high gradient of vorticity. From the time histories of α, $\frac{h}{c}$ and E_{tot} and related FFT analyses of hlade displacements, the aeroelastic behavior for the case with $V^* = 3.33$ is almost dominated by the fundamental instability. However, a significant response of frequency $\frac{6f_0}{5}$ for the plunging motion should be considered when the value of V^* is equal to 2.5. In the transonic stall flutter calculation with four hlades and $V^* = 3.33$, the unsteady behavior of shock and boundary-layer interaction is observed. The vortex-shedding first appears at the lowest blade, then it occurs at the second blade. Based on the FFT analysis of the lowest blade displacements, it is found that the aeroelastic behavior is not completely dominated by the fundamental instahility. In the study of choke flutter with $\sigma = 180°$ and $V^* = 3.33$, the computed instantaneous meshes, pressure contours and velocity vectors around the trailing edge indicate the time-variation of λ shocks with separation buhbles. From the vorticity contours, the vortex-shedding phenomenon is not observed. Based on the FFT analysis of hlade displacements, the aeroelastic behaviors are similar to those of transonic stall flutter with $\sigma = 180°$. When the transonic choke flutter of cascade with four blades and $V^* = 3.33$ is studied, the time-variation of choking flowfields within flow passages are observed. Without vortex-shedding, the regions of high gradient of vorticity are also detected. According to the time histories of α, $\frac{h}{c}$ and E_{tot}, the second blade is less unstable than the third and highest hlades. Also, the FFT analysis of lowest hlade displacements indicates that the transonic choke flutter hehavior can be determined hy the fundamental instability. From the relationship of flow phenomena to the blade displacements ($\sigma = 180°$ and $V^* = 3.33$), the hending and torsion modes should he considered simultaneously in the present stall and choke flutter problems. By using the modal identification technique and an extrapolation process, the flutter reduced velocities for the transonic stall and choke flutter of cascade with $\sigma = 180°$ are estimated.

REFERENCES

Abu-Ghannam, B. J., and Shaw, R., 1980, "Natural Transition of Boundary Layers-The Effects of Turbulence, Pressure Gradient, and Flow History," *Journal Mechanical Engineering Science*, Vol. 22, No. 5, pp. 213-228.

Bakhle, M. A., Reddy, T. S. R., and Keith, T. G., Jr., 1992, "Time Domain Flutter Analysis of Cascades Using a Full-Potential Solver," *AIAA Journal*, Vol. 30, No. 1, pp. 163-170.

Baldwin, B. S., and Lomax, H., 1978, "Thin Layer Approximation and Algebraic Model for Separated Turbulent Flows," AIAA Paper 78-257.

Bendiksen, O. O., and Hsiao, Chingteng, 1993, "New Computational Method for Aeroelastic Problems in Turbomachines, Part II," UCLA Report ENG-93-14, University of California, Los Angles.

Bennett, R. M., and Desmarais, R. N., 1975, "Curve Fitting of Aeroelastic Transient Response Data with Exponential Functions," *Flutter Testing Techniques*, NASA SP-415, pp. 43-58.

Dowell, E. H., Curtiss, H. C., Jr., Scanlan, R. H., and Sisto, F., 1989, A Modern Course in Aeroelasticity, Kluwer Academic Publishers, Dordrecht / Boston / London.

El-Aini, Y. M., Bankhead, H. R., and Meece, C. E., 1986, "Subsonic/Transonic Stall Flutter Investigation of an Advanced Low Pressure Compressor," ASME Paper 86-GT-90.

Giles, M. B., 1990, "Nonreflecting Boundary Conditions for Euler Equation Calculations," *AIAA Journal*, Vol. 28, No. 12, pp. 2050-2058.

He, L., and Denton, J. D., 1994, "Three-Dimensional Time-Marching Inviscid and Viscous Solutions for Unsteady Flows Around Vibrating Blades," *ASME Journal of Turbomachinery*, Vol. 116, pp. 469-476.

Hwang, C. J., and Fang, J. M., 1995a, "Solution-Adaptive Approach for Unsteady Flow Calculations on Quadrilateral-Triangular Meshes," AIAA Paper 95-1723.

Hwang, C. J., and Fang, J. M., 1995b, "Flutter Analysis of Cascades Using an Euler/Navier-Stokes Solution-Adaptive Approach ," Submitted to *AIAA Journal*.

Hwang, C. J., and Yang, S. Y., 1994, "Viscous Solutions for Transonic Oscillating Cascade Flows Using Dynamic Quadrilateral-Triangular Meshes," ASME Paper 94-GT-21.

Jutras, R. R., Stallone, M. J., and Bankhead, H. R., 1980, "Experimental Investigation of Flutter in Mid-Stage Compressor Designs," AIAA Paper 80-0786.

Mayle, R. E., 1991, "The Role of Laminar-Turbulent Transition in Gas Turbine Engines," *ASME Journal of Turbomachinery*, Vol. 113, pp. 509-537.

Micklow, J., and Jeffers, J., 1981, "Semi-Actuator Disk Theory for Compressor Choke Flutter," NASA CR-3426.

Reddy, T. S. R., Bakhle, M. A., Huff, D. L., and Swafford, T. W., 1991, "Flutter Analysis of Cascades Using a Two Dimensional Euler Solver," AIAA Paper 91-1681.

Siden, L. D. G., 1991, "Numerical Simulation of Unsteady Viscous Compressible Flows Applied to Blade Flutter Analysis," ASME Paper 91-GT-203.

Sisto, F., Thangam, S., and Abdel-Rahim, A., 1991, "Computational Prediction of Stall Flutter in Cascaded Airfoils," *AIAA Journal*, Vol. 29, No. 7, pp. 1161-1167.

Tanida, Y., and Saito, Y., 1977, "On Choking Flutter," *Journal of Fluid Mechanics*, Vol. 82, pp. 179-191.

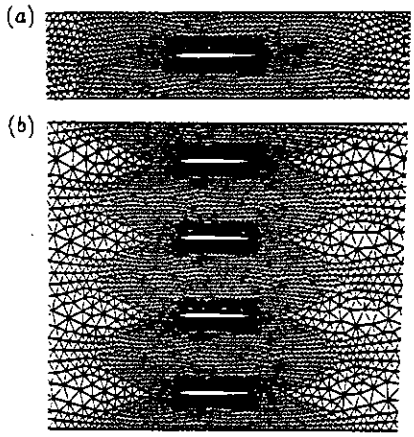

Fig. 1 Coarse meshes (background grids) in transonic stall and choke flutter calculations : (*a*) NACA 0006 cascade with $\sigma = 180°$ (4810 elements) and (*b*) NACA 0006 cascade with four blades (16630 elements).

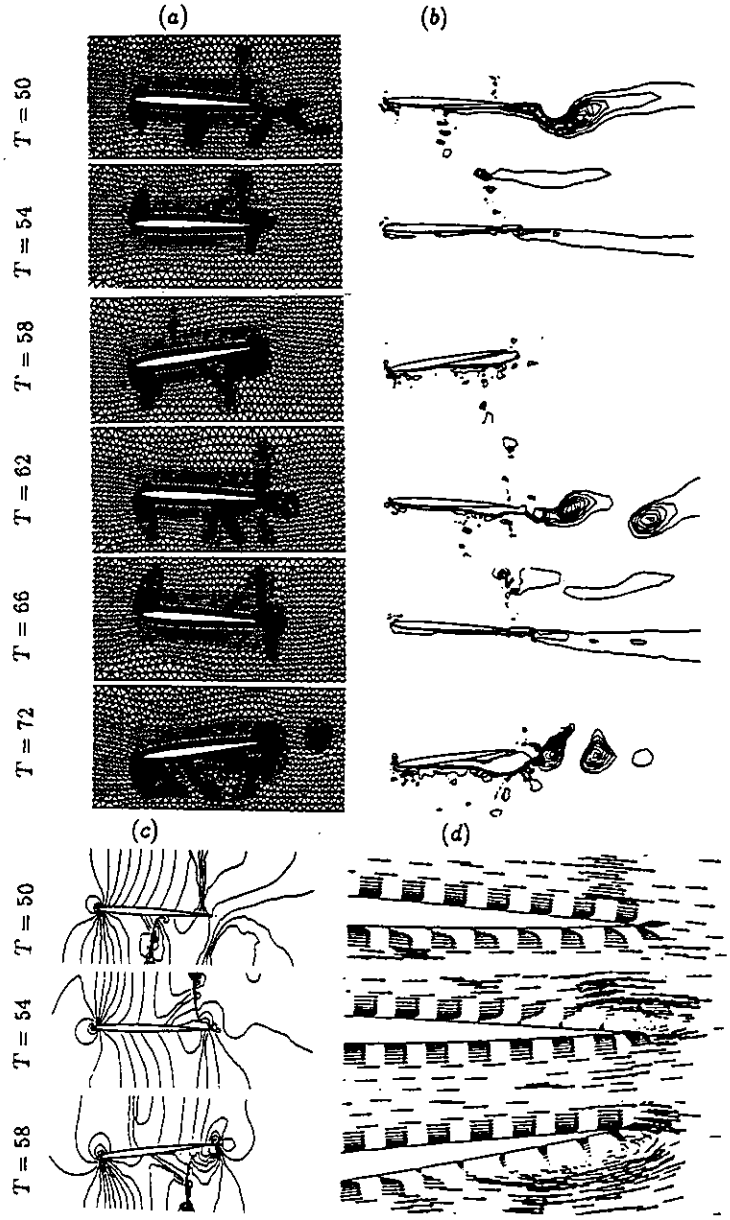

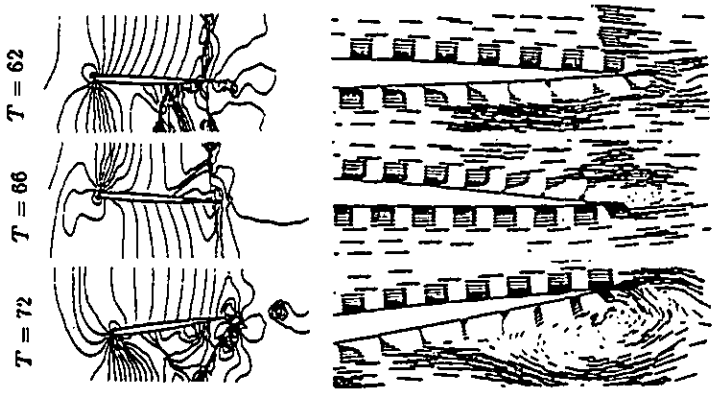

Fig. 2 The sequence of (a) instantaneous meshes, (b) vorticity contours, (c) pressure contours and (d) velocity vectors around the trailing edge at different points in time for the unstaggered NACA 0006 cascade with $\sigma = 180°$ in transonic stall flutter calculations at $V^* = 3.33$.

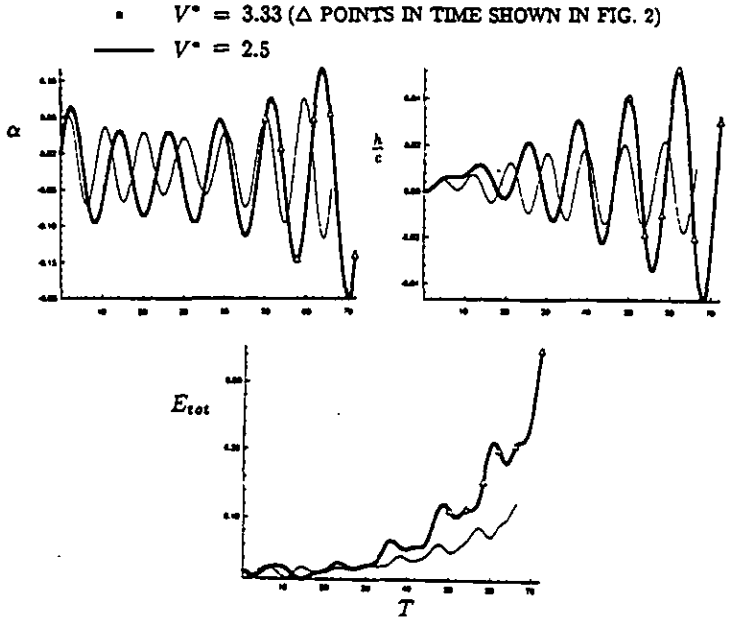

Fig. 3 Histories of α, $\frac{h}{c}$ and E_{tot} for the unstaggered NACA 0006 cascade with $\sigma = 180°$ in transonic stall flutter calculations.

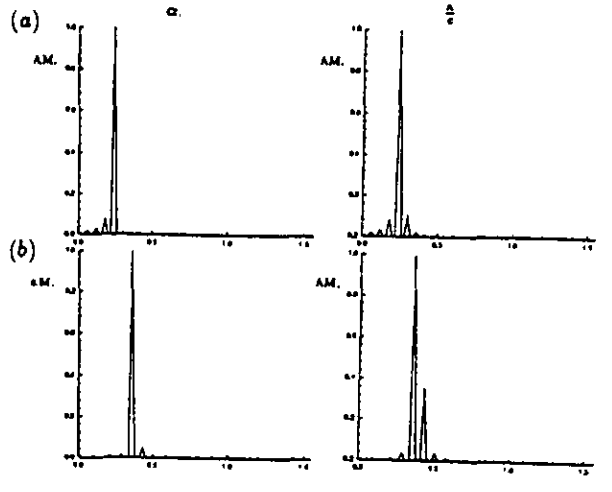

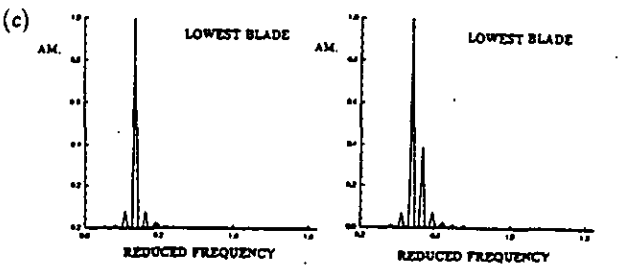

Fig. 4 Fast Fourier Transformation of blade displacements (α and $\frac{h}{c}$) in transonic stall flutter calculations : (a) cascade with $\sigma = 180°$ at $V^* = 3.33$, (b) cascade with $\sigma = 180°$ at $V^* = 2.5$ and (c) cascade with four blades at $V^* = 3.33$.

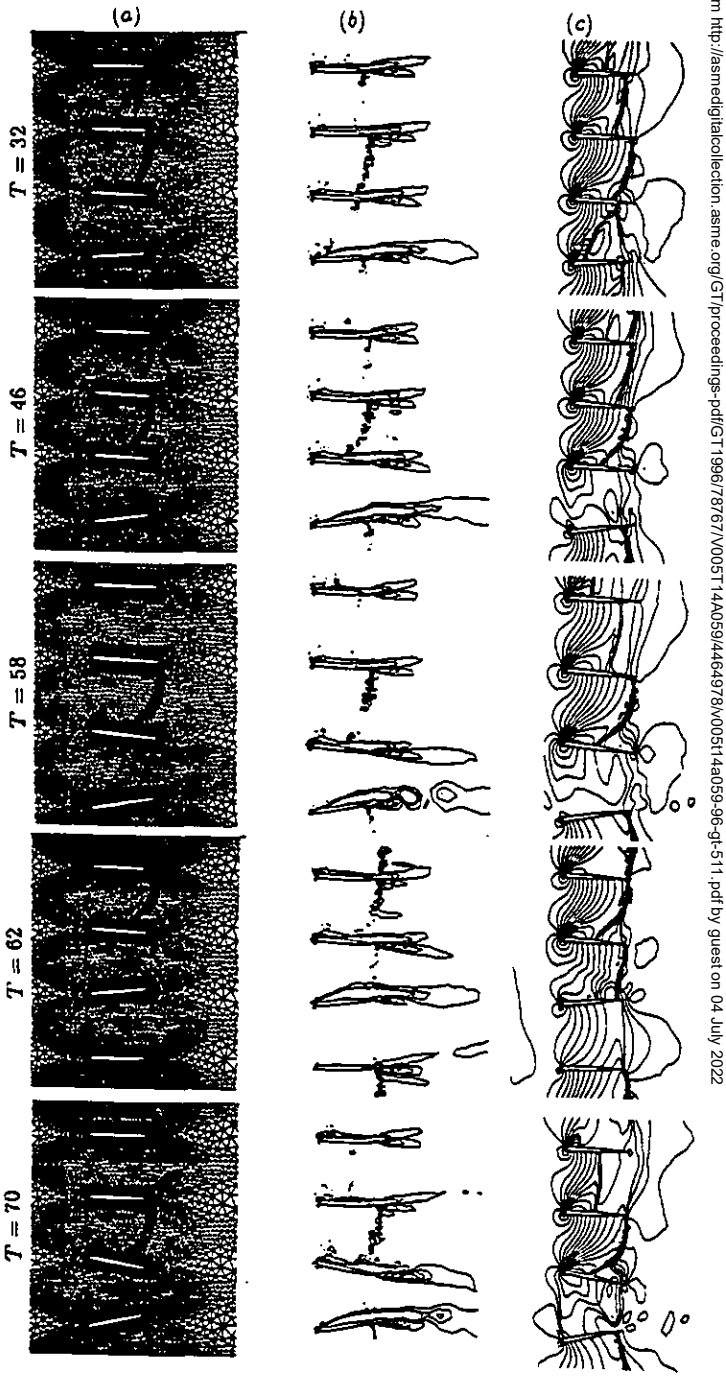

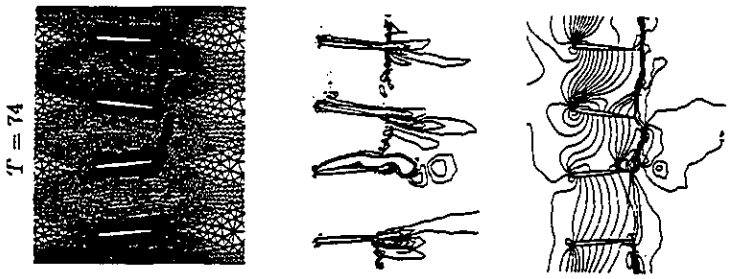

Fig. 5 The sequence of (a) instantaneous meshes, (b) vorticity contours and (c) pressure contours at different points in time for the unstaggered NACA 0006 cascade with four blades in transonic stall flutter calculations at $V^* = 3.33$.

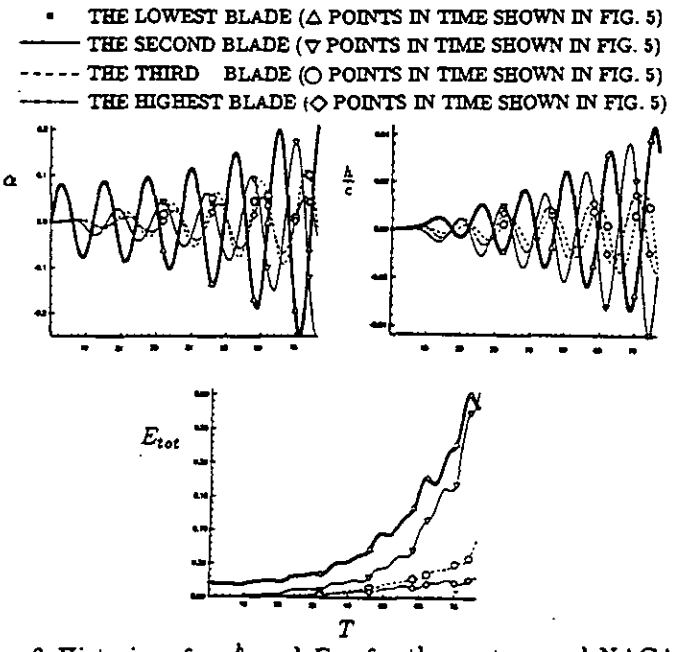

Fig. 6 Histories of α, $\frac{h}{c}$ and E_{tot} for the unstaggered NACA 0006 cascade with four blades in transonic stall flutter calculations at $V^* = 3.33$.

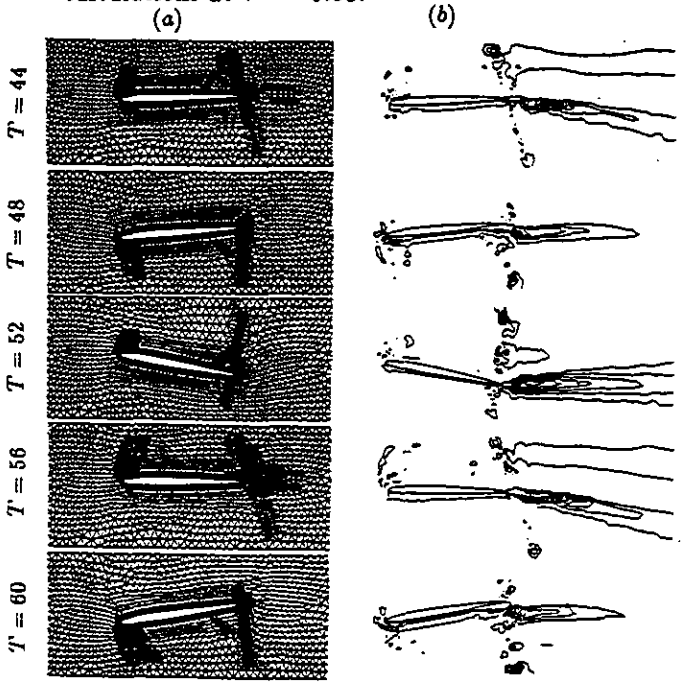

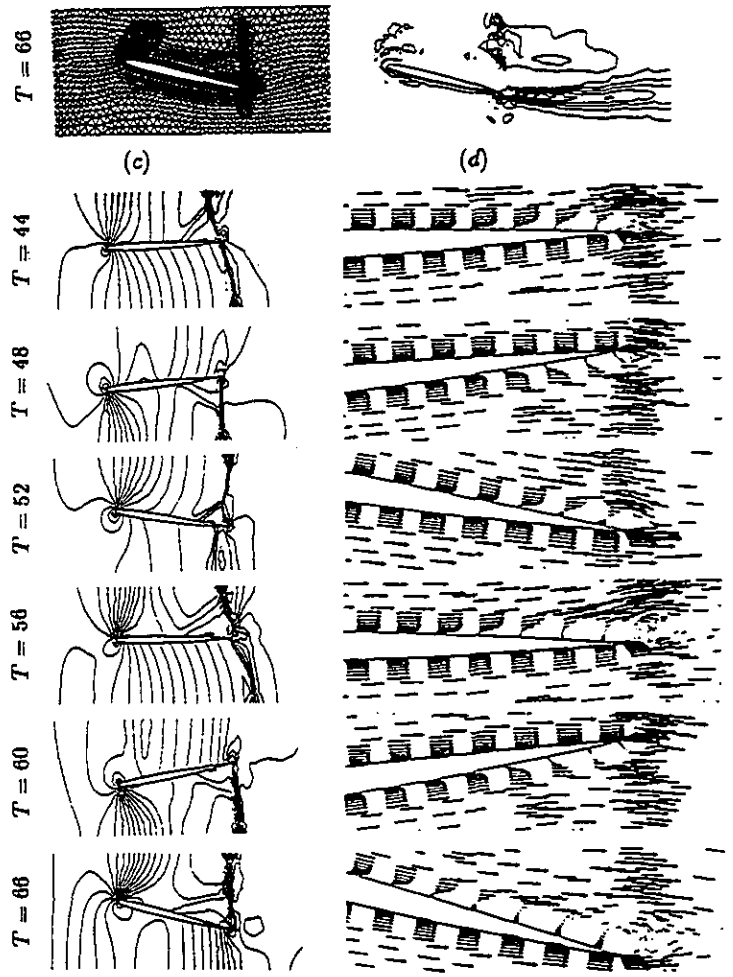

Fig. 7 The sequence of (a) instantaneous meshes, (b) vorticity contours, (c) pressure contours and (d) velocity vectors around the trailing edge at different points in time for the unstaggered NACA 0006 cascade with $\sigma = 180°$ in transonic choke flutter calculations at $V^* = 3.33$.

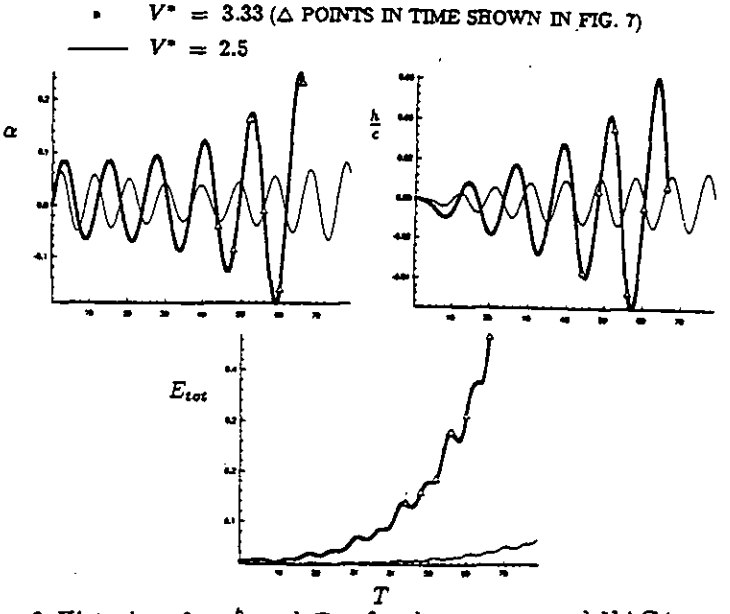

Fig. 8 Histories of α, $\frac{h}{c}$ and E_{tot} for the unstaggered NACA 0006 cascade with $\sigma = 180°$ in transonic choke flutter calculations.

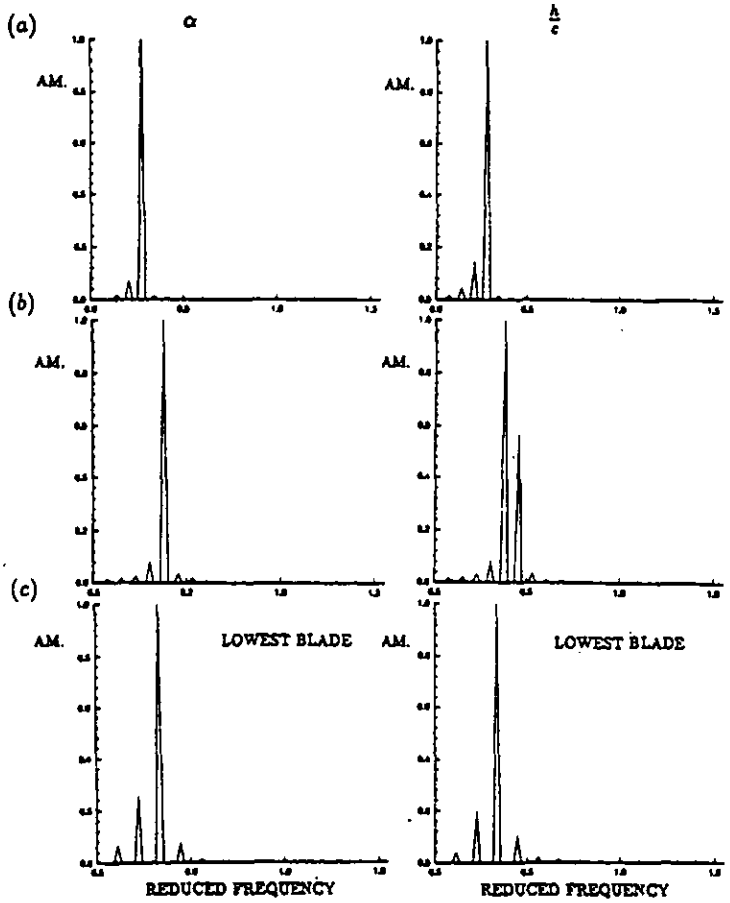

Fig. 9 Fast Fourier Transformation of blade displacements (α and $\frac{h}{c}$) in transonic choke flutter calculations : (a) cascade with $\sigma = 180°$ at $V^* = 3.33$, (b) cascade with $\sigma = 180°$ at $V^* = 2.5$ and (c) cascade with four blades at $V^* = 3.33$.

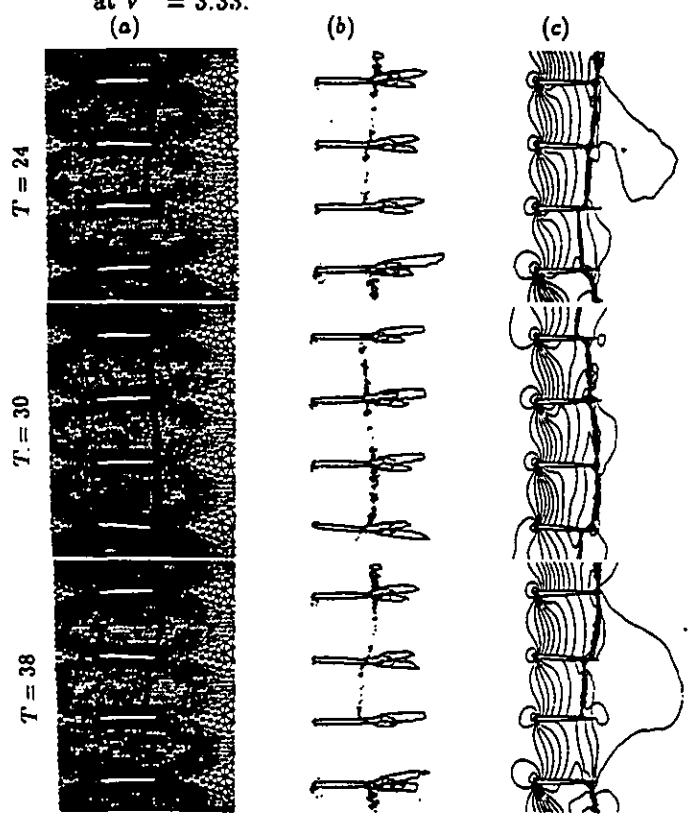

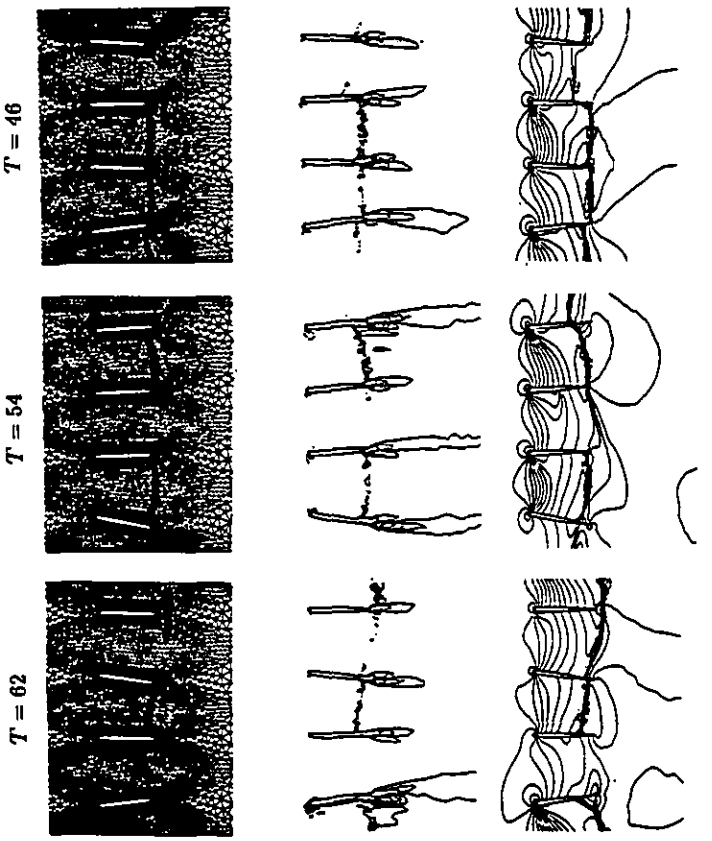

Fig. 10 The sequence of (a) instantaneous meshes, (b) vorticity contours and (c) pressure contours at different points in time for unstaggered NACA 0006 cascade with four blades in transonic choke flutter calculations at $V^* = 3.33$.

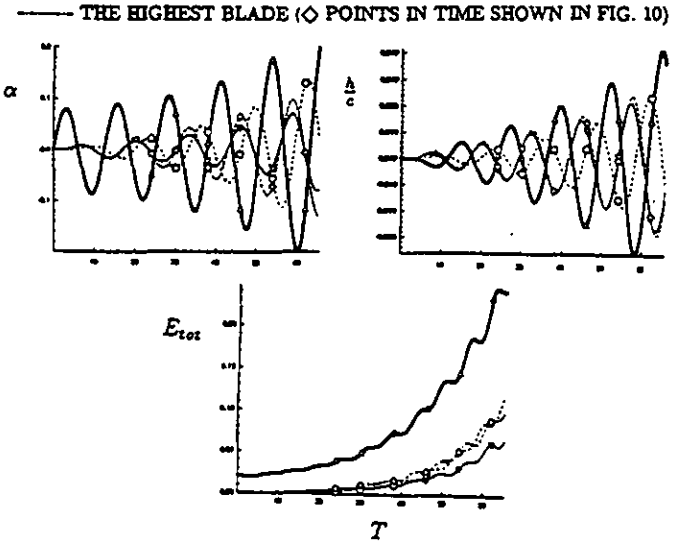

Fig. 11 Histories of α, $\frac{h}{c}$ and E_{tot} for the unstaggered NACA 0006 cascade with four blades in transonic choke flutter calculations at $V^* = 3.33$.